Neurobiology of Disease 124 (2019) 189–201

Contents lists available at ScienceDirect

Neurobiology of Disease

journal homepage: www.elsevier.com/locate/ynbdi

Inactivation of sphingosine-1-phosphate receptor 2 (S1PR2) decreases demyelination and enhances remyelination in animal models of multiple sclerosis

Maryam S. Seyedsadr[a,b], Oliver Weinmann[b,1], Ana Amorim[c], Benjamin V. Ineichen[b], Matteo Egger[b], Javad Mirnajafi-Zadeh[a], Burkhard Becher[d], Mohammad Javan[a,d,**,2], Martin E. Schwab[b,*,2]

[a] Department of Physiology, Faculty of Medical Sciences, Tarbiat Modares University, Tehran, Iran
[b] Brain Research Institute, University of Zurich, CH-8057 Zurich, Switzerland
[c] Institute of Experimental Immunology, University of Zürich, Winterthurerstrasse 190, CH-8057 Zürich, Switzerland
[d] Department Brain and Cognitive Sciences, Cell Science Research Center, Royan Institute for Stem Cell Biology and Technology, ACECR, Tehran, Iran

ARTICLE INFO

Keywords:
S1PR2 inactivation
JTE-013
Lysolecithin
Experimental autoimmune encephalitis
Blood brain barrier
Nogo-A
Oligodendrocyte progenitor cells
Myelin repair
Fibrinogen

ABSTRACT

Multiple sclerosis is an inflammatory disease of the central nervous system (CNS) in which multiple sites of blood-brain barrier (BBB) disruption, focal inflammation, demyelination and tissue destruction are the hallmarks. Here we show that sphingosine-1-phosphate receptor 2 (S1PR2) has a negative role in myelin repair as well as an important role in demyelination by modulating BBB permeability. In lysolecithin-induced demyelination of adult mouse spinal cord, S1PR2 inactivation by either the pharmacological inhibitor JTE-013 or S1PR2 gene knockout led to enhanced myelin repair as determined by higher numbers of differentiated oligodendrocytes and increased numbers of remyelinated axons at the lesion sites. S1PR2 inactivation in lysolecithin-induced demyelination of the optic chiasm, enhanced oligodendrogenesis and improved the behavioral outcome in an optokinetic reflex test. In order to see the effect of S1PR2 inactivation on demyelination, experimental autoimmune encephalitis (EAE) was induced by MOG-peptide. S1PR2 inhibition or knockout decreased the extent of demyelinated areas as well as the clinical disability in this EAE model. Both toxin induced and EAE models showed decreased BBB leakage and reduced numbers of $Iba1^+$ macrophages following S1PR2 inactivation. Our results suggest that S1PR2 activity impairs remyelination and also enhances BBB leakage and demyelination. The former effect could be mediated by Nogo-A, as antagonism of this factor enhances remyelination and S1PR2 can act as a Nogo-A receptor.

1. Introduction

Multiple sclerosis (MS) is an inflammatory disease of the central nervous system (CNS) which can lead to permanent disability depending on the type and progression of the disease. Multiple sites of focal blood brain barrier (BBB) breakdown and invasion of immune cells into the CNS are among the first pathological manifestations of MS. Subsequently, demyelination and axonal damage will occur and in the later stage of the disease, chronic demyelination, scar formation and neuronal loss are prominent. Most of the current treatments focus on controlling the immunological attack to the CNS. Therapeutic approaches for the chronic stages of MS are essentially missing at present (Ransohoff et al., 2015). Finding a reparative and regenerative approach besides preserving the CNS from immune cell invasion would greatly increase the efficiency of MS treatments (Franklin and Ffrench-Constant, 2017). Recent studies focused on compounds that enhance

Abbreviations: S1PR2, Spingosine-1-phosphate receptor 2; EAE, experimental autoimmune encephalitis; dpi, days post injection; DF, dorsal funiculus; cpd, cycles per degree; OPCs, oligodendrocyte progenitor cells; S1P, sphingosine-1-phosphate; PDGFRα, platelet derived growth factor receptor α; EdU, 5-ethynyl-2′-deoxyuridine

* Corresponding author.
** Correspondence to: M. Javan, Department of Physiology, Faculty of Medical Sciences, Tarbiat Modares University, Tehran, Iran
E-mail addresses: mjavan@modares.ac.ir (M. Javan), schwab@hifo.uzh.ch (M.E. Schwab).
[1] Present address: Institute of Veterinary Pharmacology and Toxicology, University of Zurich, Winterthurerstrasse 260, 8057 Zürich, Switzerland.
[2] Equal contribution senior authors.

https://doi.org/10.1016/j.nbd.2018.11.018
Received 6 May 2018; Received in revised form 8 October 2018; Accepted 19 November 2018
Available online 22 November 2018
0969-9961/

remyelination in animal models of MS; efficiency of such a treatment in ameliorating the visual symptoms after optic nerve inflammation in MS patients was shown recently (Deshmukh et al., 2013; Green et al., 2017; Najm et al., 2015).

Sphingosine-1-phosphate receptor 2 (S1PR2) is a G-protein coupled receptor (GPCR) with two identified ligands: Sphingosine-1-phosphate (S1P) and the neurite growth inhibitory membrane protein Nogo-A (Kempf et al., 2014). S1P is a lipid signaling molecule which mediates many physiological functions by acting through five receptors named S1PR1–5. Nogo-A is a well-studied inhibitory molecule for neurite growth in the CNS of mammals and it was shown that it's most active domain (named Nogo-Δ-20) binds with high affinity to S1PR2. Nogo-A binding to S1PR2 activates the receptor and downstream intracellular signaling, leading to actin cytoskeleton inactivation and neurite outgrowth arrest (Kempf et al., 2014). S1PR2 is expressed in many cell types including, BBB components, macrophages, and oligodendroglia progenitor cells (OPCs) (Adada et al., 2013; Novgorodov et al., 2007). The signaling pathway of both ligands, S1P and Nogo-A, through S1PR2 involves the activation of Rho-A which mediates various functions by inducing cytoskeletal changes (Kempf et al., 2014). Depending on the cell type, Rho activation can affect neurite outgrowth, barrier functions of vascular cells, and myelin formation (Laura Feltri et al., 2008; Schwab and Strittmatter, 2014).

Targeting of Nogo-A signaling pathway for enhancing reparative mechanisms in MS has been addressed in different animal models. Nogo-A inactivation by application of antibodies or by genetic manipulations could decrease the clinical disability in experimental autoimmune encephalitis (EAE) in rodents and concomitantly exert a protective effect on myelin and axons. The suggested underlying mechanisms are axonal regrowth and immune response regulation (Ineichen et al., 2017; Karnezis et al., 2004; Yang et al., 2010). In addition, in a toxin induced model of demyelination by lysolecithin injection, inactivation of Nogo-A with the same strategies increased remyelination extensively (Chong et al., 2012; Ineichen et al., 2017). Some studies were looking at the role of a second Nogo receptor, NgR1, in EAE and experimental white matter demyelination. NgR1 knockout mice showed a milder EAE due to a decrease in axonal degeneration (Petratos et al., 2012). Inactivation of NgR1 and one of the co-receptors named Lingo1 by different approaches were shown to increase the remyelination by inducing migration and differentiation of OPCs (Mi et al., 2007; Pourabdolhossein et al., 2014; Sozmen et al., 2016). Lingo1 antibody in a phase 2 clinical trial for treatment of optic neuritis in acute and chronic MS patients showed partial efficacy in certain outcome measures (Mellion et al., 2017). An interesting question, therefore, was whether also S1PR2 could have a role in repair processes after myelin lesion.

While the role of S1PR2 in animal models of MS has not been extensively studied so far, another receptor of this family, S1PR1, and its functional antagonist named FTY720 (Fingolimod) were at the center of attention based on the potent immune modulatory, disease modifying, and reparative effects of FTY720 (Brinkmann et al., 2010; Miron et al., 2010; Yazdi et al., 2015). Recently, a negative role of S1PR2 for the barrier function of the BBB was shown to influence EAE and MS; S1PR2 inactivation reduced BBB leakage and ameliorated behavioral deficits in the rodent EAE model (Cruz-Orengo et al., 2014). However, the role of S1PR2 in myelin repair has not been addressed so far.

Here we asked if S1PR2 inactivation would decrease the demyelination by modulating BBB properties. Furthermore, we hypothesized that similar to the Nogo-A receptor NgR1, S1PR2 could have a function in myelin repair. The results show that S1PR2 inactivation by the pharmacological inhibitor JTE-013 or by S1PR2 gene knockout (KO) in mice reduces BBB leakage and macrophage recruitment and increases remyelination following lysolecithin-induced demyelination. Similar results were seen in BBB integrity and macrophage recruitment in an EAE model. Positive effects of S1PR2 inactivation on BBB integrity and macrophage recruitment may explain decreased demyelination and a better clinical course in EAE mouse model of MS.

2. Methods

2.1. Animals

Adult male wild-type C57Bl/6 mice (8–12 weeks) were purchased from Charles River. Constitutive S1PR2 KO mice ($S1PR2^{tm1Rlp}$) (Kono et al., 2004) were obtained from the laboratory of R.L.Proia (National Institute of Diabetes and Digestive and Kidney Diseases, NIH, Bethesda, MD). S1PR2 KO mice were bred in our animal facility. Male KO mice were used within the same age range as the wild type mice. Animals were kept at a normal light/dark cycle with food and water ad libitum. All the experiments were performed in accordance with the guidelines of the Veterinary Office of the Canton of Zurich, Switzerland (license numbers: 119/2015 and 70/2015).

2.2. Demyelination induction by lysolecithin

In order to induce demyelination in the spinal cord, 0.5 µl lysolecithin (Sigma-Aldrich, L4129) 1% was injected into the midline of the dorsal column with a Hamilton syringe at the C4/C5 level at a depth of 300 µm down from the spinal cord surface.

Lysolecithin injection into the optic chiasm was done by stereotaxic surgery. 1 µl lysolecithin 1% was injected by injection pump with a 10 µl Hamilton syringe with the speed of 10 nanoliters per second using the following coordinates: 4.5 mm anterior to Lambda, 5.7 mm deep from the skull surface and 0 mm from the midline. The needle was kept for 5 min in place to avoid reflux.

Animals were sacrificed at 3, 7, 14 or 16 days post injection (dpi), which are critical time points for investigating BBB breakdown, demyelination, oligodendrocyte precursor cell (OPC) proliferation, and remyelination, respectively. The accuracy of targeting the optic chiasm was verified by MBP immunostaining for each individual animal; animals with no sign of demyelination were excluded from the analysis.

2.3. EAE induction

Mice were immunized subcutaneously with 200 µg of MOG peptide (amino acids: 35–55) in complete Freund's adjuvants (CFA). 200 ng pertussis toxin were administered intraperitoneally at the day of immunization and 2 days afterward. Animals were controlled daily for clinical score and body weight; they were scored as follows: 0, no detectable signs of EAE; 0.5, distal limp tail; 1, complete limp tail; 1.5, limp tail and hind limb weakness; 2, unilateral partial hind limb paralysis; 2.5, bilateral partial hind limb paralysis; 3, complete bilateral hind limb paralysis; 3.5, complete hind limb paralysis and unilateral forelimb paralysis; 4, total paralysis of fore and hind limbs (score $>$ 4, to be euthanized).

2.4. S1PR2 inhibition by JTE-013

In the lysolecithin model, daily intraperitoneal (i.p.) injections of JTE-013 (Tocris, Cat No.2392) was started immediately after the surgery and continued until sacrificing day. JTE-013 was applied every 12 h in a 15 mg/kg dose (as 1.43 mg/ml in a 1:3 solution of DMSO: H_2O). The same dose of JTE-013 was previously administrated to reduce the permeability of the BBB (Kim et al., 2015). Since measuring the plasma concentration of JTE-013 by HPLC showed its elimination at 12 h post injection (unpublished data), the dosage were divided in two injections. In the EAE experiment, JTE-013 injections were started at the day of first observation of clinical disability and continued until sacrificing day (30 mg/kg-i.p. once a day). Vehicle groups received the same amount of vehicle. There were no differences in body weight between JTE-013 treated and vehicle groups in lysolecithin model (data not shown).

2.5. EdU labelling of dividing cells

In order to investigate the effects of S1PR2 inactivation on OPC recruitment we performed EdU-pulse labelling. Alkyne attached EdU (ThermoFisher, E10187) was injected (80 mg/kg-i.p.) at 4 dpi in the lysolecithin experiments and 5 days after the first sign of clinical disability in the EAE experiments. With this short pulse of EdU we could label a fraction of proliferating cells to study the recruitment and differentiation of OPCs over time. Incorporation of EdU into DNA was visualized on the tissue sections by the CLICK-IT reaction in which a labeled azide (ThermoFisher, A10277) reacts with terminal alkynes via a copper-catalyzed reaction (Salic and Mitchison, 2008).

2.6. Measuring sensitivity of the optokinetic reflex response using the 'OptoMotry' setup

The threshold of the spatial frequency of a moving grating at which a head pursuit movement can be elicited as part of an optokinetic reflex was determined in mice with lysolecithin injections into optic chiasm using an OptoMotry setup (CerebralMechanics) (Prusky et al., 2004). Mice were placed on a platform in the middle of a virtual rotating cylinder, and full contrast rotating gratings with different frequencies were shown. Based on the optokinetic reflex, mice respond to the rotating cylinder by a head movement in same direction as the cylinder movement. The ability of the mice to respond to a specific frequency was judged by an observer blinded to the frequencies. The highest frequency which still induces a head movement response was taken as a readout of visual acuity. The values (cycles per degree (cpd)) of both eyes were recorded, averaged and compared between groups.

2.7. Tissue processing for immunohistofluorescence studies

Mice were sacrificed by transcardial perfusion with Ringer solution and 4% formaldehyde under deep anesthesia. Brain tissue and spinal cord were dissected, post fixed in formaldehyde 4% overnight and cryopreserved in 30% sucrose in 0.1 M phosphate buffer until embedding. Tissue embedding was done in OCT (Tissue-Tek, 4583), followed by freezing in Methylbutan cooled to −40 °C by liquid nitrogen; the blocks were then stored at −20 °C. Nine µm thick cross sections of the spinal cord containing the lysolecithin lesion were cut on a cryostat. For optic chiasm samples, coronal sections were prepared with 6 µm thickness, starting from the place were optic nerves merge to form the optic chiasm to the end of optic chiasm (about 1 mm). Sequential sections were collected on superfrost Plus slides. For the EAE experiments the whole spinal cord was cut in 10 µm cross sections and every 6th or 10th section was collected, Sections were mounted on slides and stored at −20 °C.

2.8. Immunohistofluorescence and image acquisition

The mounted sections were preincubated in blocking solution containing NGS 4% (normal goat serum) and TBST 0.3% (Tris buffer and 0.3% triton). This step was followed by incubation with the primary antibody overnight at 4 °C and then the incubation with a corresponding secondary antibody coupled to a fluorescent dye for 2 h at room temperature. The list of antibodies used in this experiment is provided in table 1. For MBP immunostaining antigen retrieval was done with Acetic acid/Ethanol (10 ml/190 ml) preincubation. PDGFRα (platelet derived growth factor receptor α) immunostaining for visualization of OPCs was done without any detergent, background was quenched by Sudan black staining and signal was amplified with biotinylated antibodies. Dapi or Topro3 counterstaining were used to visualize cell nuclei. In the lysolecithin experiments, for each animal the section with maximally demyelinated area was identified with MBP immunostaining and the analysis was done on this section or the adjacent section. In case of spares signals 3 adjacent sections were quantified and averaged. In the EAE tissues, based on the measurements, analysis was done on 4 to 12 sections randomly picked sections per animal corresponding to different levels of spinal cord. All the analyses and quantifications were done blindly to the experimental groups. The intensity of fibrinogen immunostaining was determined by measuring the mean gray value of the total dorsal funiculus by Image J software. Each value was normalized to the mean tissue background in gray matter and presented in relation to the values of control group. Photos were captured with an Olympus confocal microscope (fv1000), a Zeiss Axioskop microscope or a Leica SP2. Photo stitching was done by Photoshop software. Quantification of the extent of demyelinated areas and cell counting were done by Image J software.

2.9. Sudan black staining, semithin and ultrathin sectioning

Visualization of remyelinated axons was done either by Sudan black staining of thin cryostat sections as described by Ineichen et al. (2016) with some modifications, or on semithin sections stained with toluidine blue. Briefly, animals were perfused with Ringer solution and formaldehyde 4% or formaldehyde 4% + glutaraldehyde 2.5% + $CaCl_2$ and the dissected spinal cords were post fixed in the same solution for 1–5 days. In some experiments, the upper half of the lesion was used for Sudan black staining and the lower half was post fixed in osmium and processed for plastic embedding for semithin or ultrathin sectioning.

For Sudan black staining, 6 or 9 µm thick serial cryostat sections of the lesion were prepared. In experiments without glutaraldehyde perfusion, sections were postfixed with 2% glutaraldehyde in 0.1 M PB for 20 min. Sudan black staining was done with 1% Sudan black (Sigma, 199,664) in ethanol for 15 min. Remyelinated axons were defined as axons with disproportionally thin myelin as compared to their axon diameter (Duncan et al., 2017). They were counted in a 50 × 50 µm (2500 μm^2) frame centered on the lesion border by a blind investigator. The values of three sections per animal were averaged.

In order to visualize remyelinated axons on semithin and ultrathin sections, spinal cord tissue ($n = 3$ animals per group) comprising the lesion was embedded in epoxy resin and 1 µm semithin sections or 100–200 nm EM sections were cut with a diamond knife. Semithin sections were stained with 0.25% toluidine blue and electron microscopy done without contrasting using a Zeiss 10 transmission electron microscope.

In order to calculate the g-ratio (the ratio of the bare axon diameter to axon plus myelin diameter), semithin sections were visualized and pictures captured from the lesion borders in a blind fashion. For each animal three pictures were taken from three sections. The frequency of remyelinated axons and g-ratios of these axons were quantified in a 50 × 50 µm square. In this way at least 150 axons were analyzed for each animal.

2.10. Statistical analysis

Statistical analysis was performed using GraphPad Prism. In order to compare JTE-013 treated animals or S1PR2 KO animals with the control, two tailed unpaired Student's *t*-test was used. In order to compare the groups with the factor of time, multiple comparisons were used by Two-way repeated measured ANOVA with Bonferroni post-hoc correction. In Fig. 2G, two outliers were removed from vehicle group as recommended by the ROUT test. All data are presented as means ± SEM.

3. Results

3.1. The effects of S1PR2 inactivation on BBB disruption and extravasation of immune cells in the dorsal funiculus of mouse spinal cord

In order to study the effect of S1PR2 on demyelination, we first analyzed the effect of S1PR2 inactivation on BBB permeability.

Table 1
List of primary and secondary antibodies used in this study.

Primary antibody	Supplier	dilution	Secondary antibody
MBP	Millipore (AB980)	1/250	Goat anti rabbit Alexa 488 1/1000
APC (CC1)	Millipore (OP80)	1/300	Goat anti mouse Alexa 546 1/1000
PDGFRα	Cell Signaling (D1E1E)	1/250	Goat anti rabbit Alexa 488 1/1000
Fibrinogen	Dako (A0080)	1/200	Goat anti rabbit Alexa 488 1/1000
Arginase	Santa Cruz (sc-18354)	1/50	Donkey anti goat 488 1/300
CD16/32	BD pharmingen (553141)	1/100	Goat anti rat Cy3 1/1000
CD31	BD pharmingen (550274)	1/50	Goat anti rat Cy3 1/1000
S1PR2	Santa Cruz	1/100	Goat anti mouse Cy3 1/1000
Iba1	Wako (019-19741)	1/500	Donkey anti rabbit TRITC 1/500 Goat anti rabbit Alexa 488 1/1000

Vascular endothelial cells of the CNS express S1PR2 in high amounts (Fig. 1 B) and this receptor is known to contribute to the BBB barrier properties (Cruz-Orengo et al., 2014). Lysolecithin is known to increase the permeability of endothelial cells' tight junctions and to facilitate the migration of immune cells (Huang et al., 2007; Qiao et al., 2006). We, therefore, evaluated how S1PR2 inactivation by the well characterized, selective antagonist JTE-013 (Osada et al., 2002) or the absence of S1PR2 in the respective KO mice affects the BBB permeability at the sites of local injections of lysolecithin in the dorsal funiculus as indicated in schematic diagram Fig. 1 A. The extent of BBB permeability was assessed by quantifying extravasated fibrinogen immunoreactivity in the tissue. This parameter is particularly relevant as the presence of fibrinogen in CNS has been shown to initiate and augment demyelination (Ryu et al., 2015). Fibrinogen immunoreactivity was prominent at three days after lysolecithin injection (3 dpi) within and around the injection site, especially around blood vessels (Fig. 1 C). It declines over time (Sup. Fig. 1 A–C). At 3 dpi the relative optical density of fibrinogen in the dorsal funiculus was significantly reduced in JTE-013 treated as well as in the S1PR2 KO groups in comparison to the vehicle injected group ($p < .01$ and $p < .05$; Fig. 1 E and F).

BBB leakage may facilitate the infiltration of immune cells. Following lysolecithin injection, microglia and bone marrow derived macrophages were the most prominent immune cells in lysolecithin lesions (Fig. 1D) (Rawji and Yong, 2013). Therefore, we assessed the number of macrophages by Iba1 marker staining at their accumulation areas. At 3 dpi, the number of Iba1$^+$ cells was significantly decreased by about 26% in JTE-013 treated and by about 48% in the S1PR2 KO groups in comparison to the vehicle group (Fig. 1G and H; $p < .05$ and $p < .01$, respectively). Microglia and macrophages also express S1PR2 (Sup. Fig. 2C). Therefore, we assessed the inflammatory state of the intra- and perilesional microglia/macrophages by using CD16/32 as a marker for the proinflammatory, and arginase1 as a marker for the anti-inflammatory state of these cells (Miron et al., 2013). Quantifying the density of Iba1 and Arginase1 double positive cells as well as the density of Iba1 and CD16/32 double-positive cells in the lysolecithin injected dorsal funiculus revealed no significant differences between vehicle, JTE013 and S1PR2 knockout groups (Sup. Fig. 2). These results shows that the S1PR2 inactivation decreases the macrophage burden in the demyelinating lesion, however, does not change the inflammatory state of them.

Since macrophages and fibrinogen extravasation can both augment demyelination (Ryu et al., 2015), we assessed the extent of the demyelinated area at 3 dpi. At 3dpi,lysolecithin injection into white matter induced demyelination and myelin debris accumulation which was reflected by an overall decrease in MBP immunostaining as well as a sharp signal of granular, MBP-positive fragments, respectively (Sup. Fig. 1D–F). In these lysolecithin lesions, the extent of demyelination as shown by MBP staining showed no significant differences between vehicle, JTE-013 treated and S1PR2 knockout animals at 3 dpi (Fig. 1 I and J). The intensity of MBP signals was quantified in the demyelinated tissue. Similar to the extent of demyelination, no significant differences were observed for the proportion of demyelinated tissue between control, JTE-013 treated and S1PR2 KO animals group (Sup. Fig. 3). This observation suggests that in this model the extent of demyelination is mainly determined by the direct disruption of the myelin membranes by the detergent properties of lysolecithin.

3.2. The effects of S1PR2 inhibition or deficiency on oligodendrocyte precursor recruitment and oligodendrogenesis

Following lysolecithin injection, differentiation of OPCs is known to take place at 7–14 dpi and remyelination is detectable after 14 dpi (Wegener et al., 2015). We therefore asked whether S1PR2 inactivation in JTE-013 treated or S1PR2 KO groups could affect the OPCs response at 7 dpi and the level of oligodendrogenesis and remyelination at 16 dpi. At 7 dpi, OPCs were visualized by immunostaining for their marker platelet derived growth factor receptor alpha (PDGFRα) and counted in the dorsal funiculus (Fig. 2A). The newly generated OPCs were labeled by a systemic injection of EdU at 4 dpi, the peak time of OPC proliferation following lysolecithin injection (Ferent et al., 2013). About 10% of the PDGFRα$^+$ OPCs were labeled by EdU at 7 dpi (Fig. 2A arrows). We observed no significant differences neither in the total number of PDGFRα$^+$ cells nor in the PDGFRα$^+$/EdU$^+$ OPCs between the experimental groups (Fig. 2B and C). These results seem to exclude an effect of S1PR2 on OPC proliferation and short term survival.

In order to investigate the differentiation potential of OPCs to mature oligodendrocytes in the different treatment groups, immunostaining against CC1 as a marker for mature oligodendrocytes was done at 16 dpi. At the border of the lesion, some axons with relatively thin MBP$^+$ myelin sheaths were detectable adjacent to newly formed EdU$^+$/CC1$^+$ oligodendrocytes (Fig. 2D, right upper panel). As these myelin sheaths were thinner in comparison to the myelin sheath in the intact part of the dorsal funiculus (Fig. 2D, right lower panel), they could represent newly formed myelin sheaths. We quantified the number of differentiated, EdU$^+$/CC1$^+$ oligodendrocytes in the dorsal funiculus. At 16 dpi, the number of EdU$^+$/CC1$^+$ cells in JTE-013 treated and S1PR2 KO animals showed a significant increase by about 40% and 54%, respectively, in comparison to controls (both $p < .05$, Fig. 2E). To further assess the differentiation of OPCs, we calculated the ratio between labeled mature oligodendrocytes and EdU labeled, newly generated OPCs (Fig. 2F). In all experimental groups the number of EdU labeled OPCs in the dorsal funiculus dropped from 7 dpi to 16 dpi (from 13.2 ± 2.4 to 4.1 ± 1.02 cells in vehicle, from 14.2 ± 2.5 to 4.8 ± 0.8 in JTE-013 treated, and from 8.7 ± 1.1 to 3.2 ± 1.2 in S1PR2 KO animals) showing the pronounced differentiation of the OPCs to mature oligodendrocytes in this time period. At 16 dpi, we observed a significant difference of 52% in the ratio of differentiated oligodendrocytes to newly generated OPCs in S1PR2 KO mice in comparison to vehicle injected mice. This ratio also showed an increasing trend in JTE-013 treated mice (Fig. 2G). These data indicate that S1PR2 has a negative regulatory role for OPC differentiation.

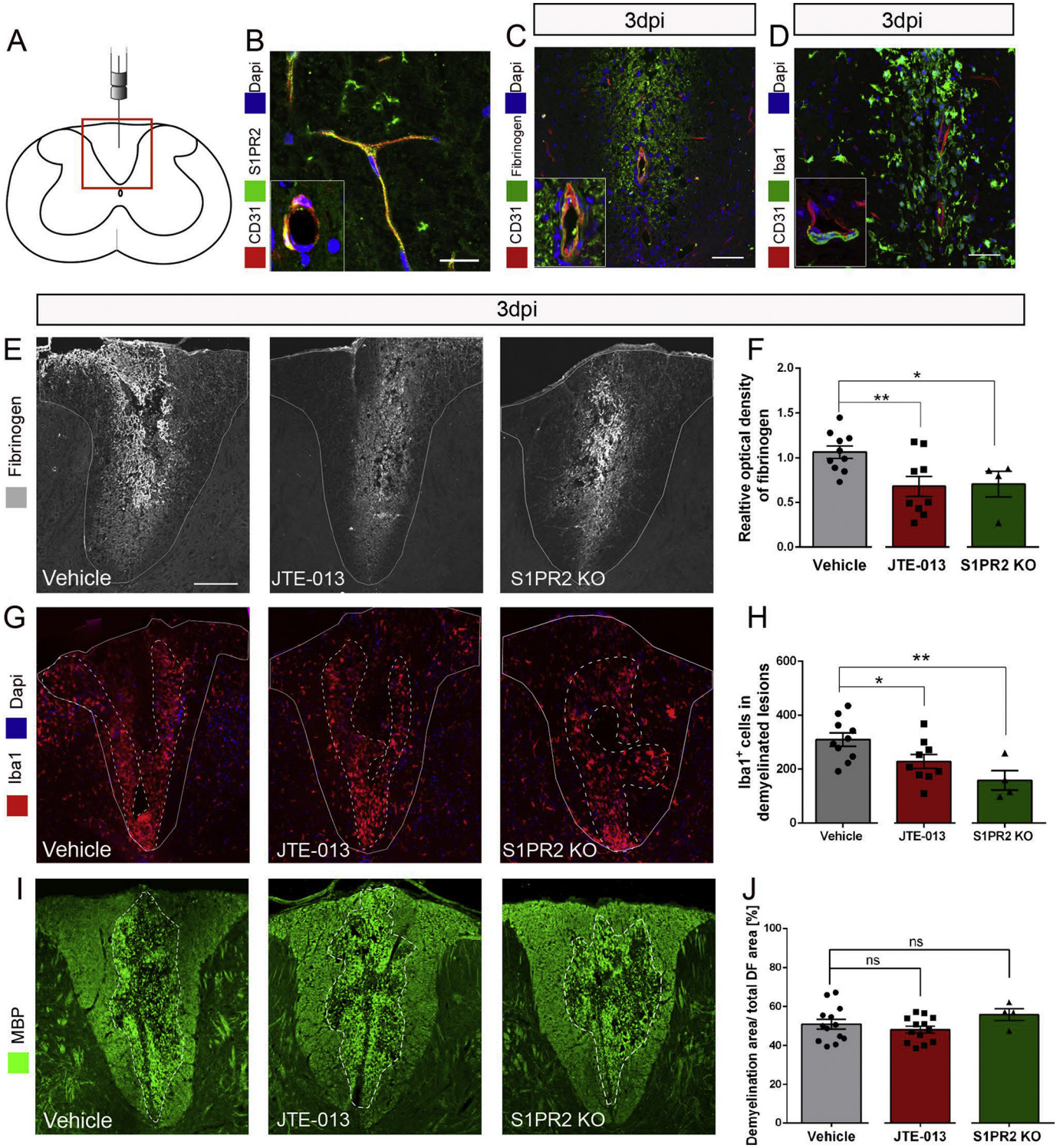

Fig. 1. S1PR2 inactivation decreases fibrinogen extravasation and inflammatory cell number, but has no effect on demyelination volume after lysolecithin injection into the dorsal funiculus. A, Dorsal funiculus (square) and injection site in C4/C5 segments of the mouse spinal cord. B, double-immunostaining for S1PR2 and the blood vessel marker CD31 shows the expression of S1PR2 in vessels in healthy animals and following EAE induction (inset) (scale bar = 20 μm). C and D, Fibrinogen and Iba1 immunostaining show BBB breakdown and recruitment of microglia/macrophages in the dorsal funiculus at 3 dpi (scale bar = 50 μm). E and F, The intensity of the fibrinogen immunostaining compared between groups in dorsal funiculus of the most demyelinated section (* $p < .05$ and ** $p < .01$, $n = 10$ for vehicle, $n = 9$ for JTE-013 treated mice, and $n = 4$ for S1PR2 KO mice, student's *t*-test). The border of dorsal funiculus is indicated by a white line. G and H, The number of Iba1 positive cells per section in accumulated area (white dotted line) compared between treatment groups in the dorsal funiculus at the level of the most demyelinated section (* $p < .05$ and ** $p < .01$, $n = 10$ for vehicle, n = 9 for JTE-013 treated mice, and $n = 4$ for S1PR2 KO mice, student's *t*-test). I and J, The demyelination area (white dotted line) determined by the presence of myelin debris compared between treatment groups (non-significant, $n = 13$ for vehicle, n = 13 for JTE-013 treated mice, and n = 4 for S1PR2 KO mice, student's *t*-test). Scale bar for E, G, and I is equal to 150 μm. Abbreviations: dpi = days post injection, DF = dorsal funiculus, ns = non-significant.

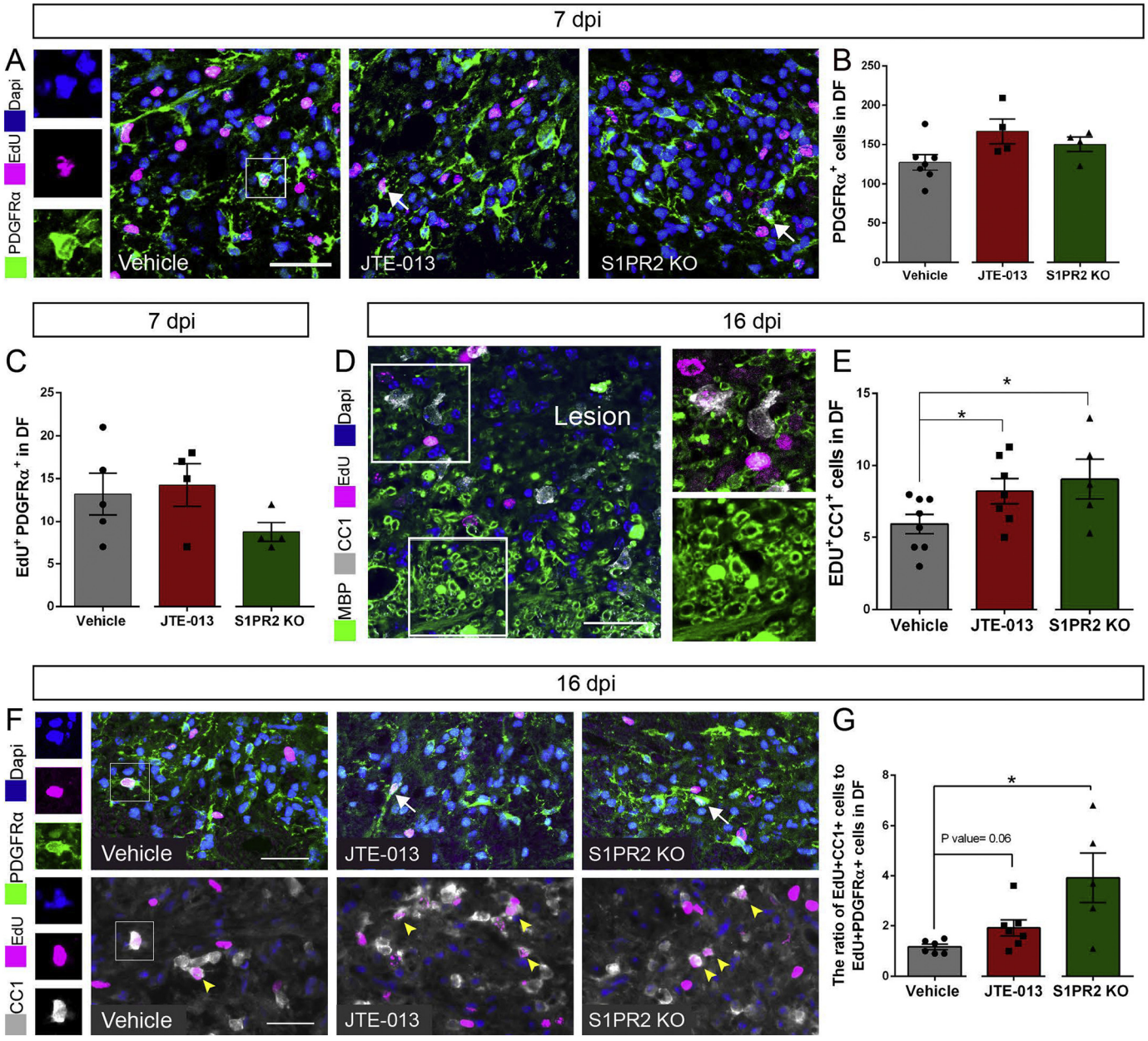

Fig. 2. S1PR2 inactivation increases OPCs differentiation but it has no effect on proliferation or recruitment. A, At 7 dpi PDGFRα $^{+}$ cells can be found abundantly in and around the demyelinated lesion and some of them are labeled with EdU (arrow) which were injected at 4 dpi (scale bar = 40 μm). B and C, The graphs show the quantification of PDGFRα^{+} cells and EdU incorporated PDGFRα^{+} cells in the dorsal funiculus of the maximally demyelinated section, at 7 dpi. D, At 16 dpi, newly formed mature oligodendrocytes (EdU^{+}/CC1^{+}) can be found at the lesion border (scale bar = 30 μm). Most of them are surrounded by thinly myelinated axons (right panel up, 45 μm × 45 μm) which is different from the intact myelin (right panel down, 45 μm × 45 μm). E, The graph compares the number of newly formed oligodendrocytes as indicated by CC1 and EdU staining for groups at 16 dpi (the average of three sections, * $p < .05$, $n = 8$ for vehicle, $n = 7$ for JTE-013 treated mice, and $n = 5$ for S1PR2 KO mice, student's *t*-test). F, Upper panels show the EdU^{+}/PDGFRα^{+} cells (white arrows) and lower row shows EdU^{+}/CC1^{+} cells (yellow arrow heads) in the demyelinated lesion at 16 dpi (scale bar = 30 μm). G, The graph shows the ratio of EdU labeled oligodendrocytes to EdU labeled OPCs, at 16 dpi (* p < .05, $n = 6$ for vehicle, n = 7 for JTE-013 treated mice, and n = 5 for S1PR2 KO mice, student's *t*-test). For A and E, The separate colour channels were shown for the single cell located in the white square. Abbreviations: dpi = days post injection, DF = dorsal funiculus. (For interpretation of the references to colour in this figure legend, the reader is referred to the web version of this article.)

3.3. The effect of S1PR2 inactivation on myelin repair

In order to study remyelination at 16 dpi, we used Sudan black staining on frozen sections (Ineichen et al., 2016) as well as the classical toluidine blue staining on semithin plastic sections of the lysolecithin demyelinated mouse dorsal funiculus. As the mature oligodendrocytes were mainly present in an about 50 μm wide band at the rims of lesions (Fig. 3 A), the number of remyelinated axons was determined in this area (Fig. 3 B and D). The quantifications based on Sudan black staining showed that in JTE-013 treated and S1PR2 KO mice, the numbers of remyelinated axons were increased by 2.09 and 2.3 folds, respectively, in comparison to the vehicle group (Fig. 3C). We also quantified the number of remyelinated axons in Nogo-A KO animals exposed to the same lysolecithin challenge using Sudan black stained sections. In line with a previous report (Chong et al., 2012) we observed a massive, 2.7 fold, increase in remyelination (data not shown). In semithin sections, the percentage of remyelinated axons over the total number of axons showed a significant increase in the JTE-013 treated group in

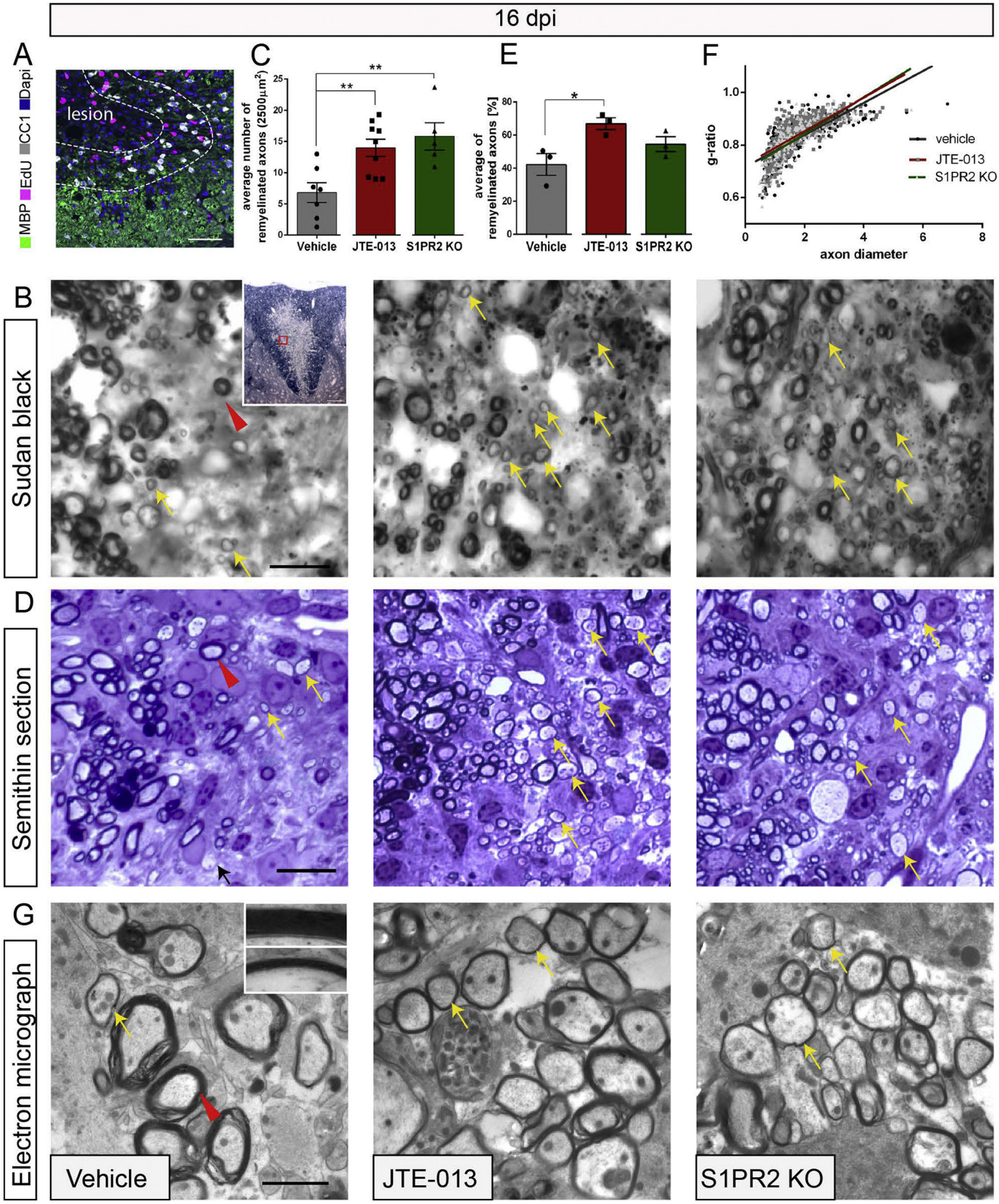

(caption on next page)

Fig. 3. Remyelination increases in JTE-013 treated and S1PR2 KO groups at 16 dpi. A, Immunostaining showing that mature oligodendrocyte ($CC1^+$ cells) are mostly found in the lesion border (scale bar = 50 μm). B, Sudan black stained frozen sections of the lesion border in the 3 treatment groups. Intact axons (red arrow heads) and many thinly remyelinated axons (yellow arrows) are present near the borders of the lesion. The inset in left image is the Sudan black staining of the dorsal funiculus. Intact myelin stained dark blue while the lysolecithin-induced demyelination is obvious in the center. The red square corresponds to the counting areas. C, Quantification of the number of remyelinated axons with Sudan black staining. (** $p < .01$, n = 7 for vehicle, n = 9 for JTE-013 treated mice, and n = 5 for S1PR2 KO mice, student's *t*-test). D, Toluidine blue staining on semithin sections showing intact axons, remyelinated axons as well as the demyelinated axons (black arrow). E, The percentage of remyelinated axons over total axons. (* $p < .05$, $n = 3$ per group, student's *t*-test). F, The scatter plot is showing the g-ratios against axonal diameter and the best-fitted line for each treatment group (n = 3 per group, linear regression). G, Representative images from electron microscopy show a higher proportion of remyelinated axons (yellow arrows) in the JTE-013 and the S1PR2 KO groups. The upper and lower inset show an intact and a remyelinated axon, respectively, at high magnification. Scale bar for Sudan black and semithin sections is equal to 10 μm and for EM images is equal to 2 μm. Abbreviation: dpi = days post injection. (For interpretation of the references to colour in this figure legend, the reader is referred to the web version of this article.)

comparison to vehicle ($p < .05$) and likewise an increasing trend in S1PR2 KO group (Fig. 3 D and E). In order to study the remyelination in more detail, g-ratios were determined for remyelinated axons in the same area in which remyelination frequency was studied. In Fig. 3 F, g-ratios are plotted against the related axonal diameter and the slope of the best-fitted line was calculated (0.060 ± 0.002 for the vehicle group, 0.063 ± 0.002 for the JTE-013 treated group and 0.068 ± 0.003 for S1PR2 KO group). The non-significant difference between the slopes indicates that in spite of the enhanced remyelination, our treatments had no effect on the myelin thickness following remyelination.

The promoting effect of S1PR2 inactivation on remyelination was also obvious in electron microscopic images from these groups, showing higher numbers of axons with thin myelin as related to the axonal diameter (Fig. 3 G). All these data show a pronounced effect of S1PR2 antagonism or deletion on remyelination in lysolecithin-induced white matter lesions of the spinal cord.

3.4. The effects of S1PR2 inactivation on lysolecithin induced optic nerve demyelination and function

Demyelination of optic nerves and chiasm and disturbed visual functions are frequent and often initial symptoms in MS patients. We therefore injected lysolecithin directly into the optic chiasm of adult mice (Fig. 4 F). Demyelination was prominent in and around the injection site at 3 dpi, as shown by MBP immunostaining (Fig. 4 A). Like in the spinal cord, no significant difference in the size of demyelinating lesions between JTE-013 and vehicle injected mice could be observed on 3 dpi (Fig. 4 B).

As a key reparative process, we analyzed the differentiation of newly proliferated OPCs, labeled by a pulse of EdU at day 4 after lesion, to $CC1^+$ oligodendrocytes (Fig. 4 C and D). The number of $CC1^+/EdU^+$ double-labeled oligodendrocytes in the optic chiasm at 14 dpi was significantly increased in the JTE-013 treated group and showed an increasing trend in S1PR2 KO animals in comparison to the vehicle injected group ($p < .05$; Fig. 4 E). These results point to enhanced conditions for remyelination after S1PR2 antagonisms also in the optic nerve.

Visual acuity-measured as sensitivity to spatial frequency in an optokinetic response task- was used to test the functionality of the lesion affected optic system (Fig. 4 G). The visual acuity dropped at 3 dpi (0.37 ± 0.006 cpd for pooled data) in comparison to baseline (0.42 ± 0.004 cpd, $p < .0001$). There were no statistically significant differences between the groups at 3 dpi (Fig. 4 H). At 14 dpi, the visual acuity recovered to some extent probably due to the remyelination-(from 0.37 ± 0.006 cpd at 3 dpi to 0.39 ± 0.005 cpd at 14 dpi for pooled data, $p < .01$). At this time point the visual acuity was significantly higher in S1PR2 KO animals when compared to vehicle treated animals ($p < .05$; Fig. 4 H).

3.5. The effects of S1PR2 inactivation on the course of experimental autoimmune encephalitis (EAE), lesion size, BBB leakage, macrophage recruitment and oligodendrocyte differentiation

With its multiple, inflammatory, autoimmune lesions, EAE resembles several features of the pathophysiology of human MS. We, therefore, studied the effects of S1PR2 inactivation on disease clinical course, BBB permeability, demyelination and remyelination processes in a MOG-peptide induced mouse EAE model. The daily JTE-013 or vehicle injections were started at the day of disease onset. This administration of JTE-013 decreased the severity of the clinical scores (Fig. 5A); the means became statistically different at days 17–18 ($p < .001$ and $p < .05$, respectively). In S1PR2 KO mice clinical scores were significantly lower than in wild type littermates at day 18 ($p < .05$; Fig. 5B). MBP immunostaining of different parts of the spinal cord revealed that the areas of the demyelinated lesions were significantly smaller in JTE-013 treated mice as well as in S1PR2 KO mice in comparison to the related control groups ($p < .05$ and $p < .01$, respectively; Fig. 5 C and D). The area of BBB leakage as determined by fibrinogen extravasation was also decreased in both JTE-013 treated and S1PR2 KO mice (both $p < .05$, Fig. 5 E and F).

We evaluated the recruitment of $Iba1^+$ macrophages/microglia in EAE spinal cords and its modulation by S1PR2 inactivation. At 18–19 days post immunization, large numbers of $Iba1^+$ cells accumulated within the inflammatory lesions, which were distributed in the white matter throughout the spinal cord (Fig. 6 G). The areas of $Iba1^+$ cell accumulations were measured on sections of spinal cord tissue of EAE mice. In S1PR2 KO mice the extent of these areas was smaller compared to wild type controls ($p < .05$), and it showed a decreasing trend in JTE-013 treated animals in comparison to the vehicle injected group (Fig. 6H).

In order to see the possible changes in oligodendrogenesis in the EAE model, we injected EdU at 5 days after the onset of disease symptoms to label newly formed oligodendrocyte lineage cells. JTE-013 treated mice had a trend to higher numbers of newly differentiated oligodendrocytes i.e. $EdU^+/CC1^+$ cells in the spinal cord (Fig. 5 I and J).

Altogether, compared to control animals treatment with JTE-013 and S1PR2 KO animals showed lower clinical disability scores, i.e. a milder disease course, less BBB leakage, less demyelination, reduced phagocyte recruitment, and increased numbers of newly generated, possibly reparative oligodendrocytes.

4. Discussion

Our results showed that key events of neuroinflammation and repair after demyelinating lesions are influenced by S1PR2: 1) BBB leakage, inflammatory cell recruitment, and demyelination, which are all decreased by inactivation of S1PR2, and 2) differentiation of newly generated oligodendrocytes and myelin repair, both of which are enhanced by inactivation of S1PR2. S1PR2 inactivation was achieved by the pharmacological antagonist JTE-013 or by genetic deletion (S1PR2 KO mice). In the model of lysolecithin induced demyelination of the dorsal funiculus of the mouse and in a similar way in the EAE model,

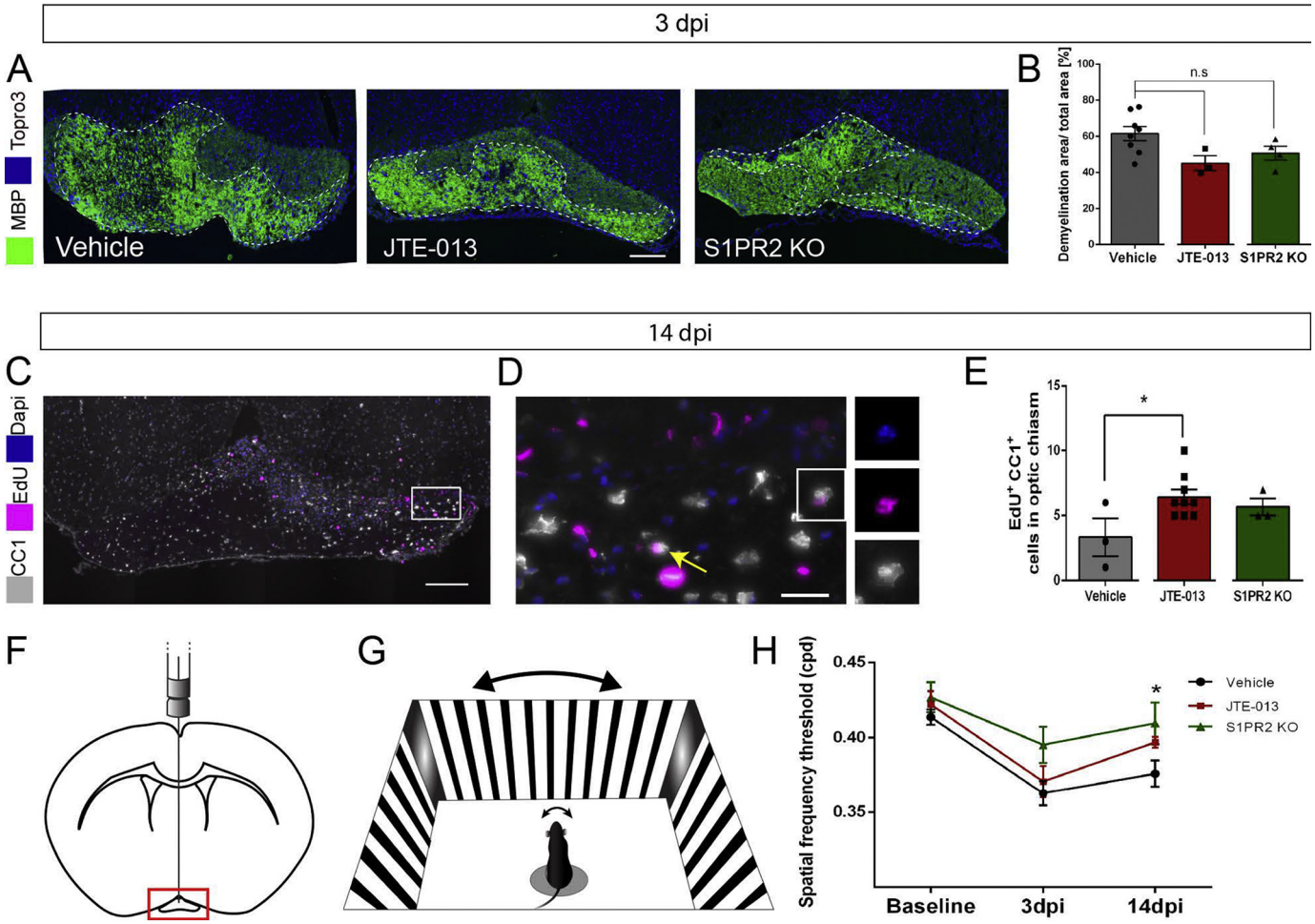

Fig. 4. S1PR2 inactivation enhances OPC differentiation and recovery of optokinetic reflex after lysolecithin injection into optic chiasm. A and B, The percentage of demyelination area (dotted line) vs. the total area of optic chiasm was quantified by MBP immunostaining at 3 dpi (scale bar = 150 μm). C and D, Overview (C) and a zoom-in picture (D) for $CC1^+/EdU^+$ immunostaining in the optic chiasm at 14 dpi. The yellow arrow points to a $CC1^+/EdU^+$ cell. The separate colour channels were shown for the single cell located in the white square in D. scale bar for C and D is equal to 150 μm and 25 μm, respectively. E, Quantification of $CC1^+/EdU^+$ cells in the optic chiasm in the vehicle, JTE-013 treated and the S1PR2 KO mice at 14 dpi (* $p < .05$, n = 3 for vehicle, n = 9 for JTE-013 treated mice, and n = 3 for S1PR2 KO mice, student's *t*-test). F, The position of optic chiasm and injection site in a schematic coronal section of the brain. G, The OptoMotry set up was used to measure the threshold of the spatial frequency at which an optokinetic response could be reliably elicited. H, The drop and recovery of visual acuity in different groups were quantified by measuring the threshold of spatial frequency in cycles per degree (cpd) of the visual field in the OptoMotry setup (* $p < .05$, n = 8 for vehicle and JTE-013 treated groups and n = 6 for S1PR2 KO group, repeated measured two-way ANOVA with Bonferroni post test). Abbreviations: dpi = days post injection, cpd = cycles per degree. (For interpretation of the references to colour in this figure legend, the reader is referred to the web version of this article.)

fibrinogen extravasation as a measure of BBB opening was decreased in JTE-013 treated and in the S1PR2 KO mice. In both lysolecithin and EAE lesions, S1PR2 inactivation decreased the recruitment of $Iba1^+$ macrophages/microglia. Importantly, both interventions also increased the differentiation of OPCs to oligodendrocytes. Due to the well-defined conditions in the lysolecithin model, remyelination could be studied quantitatively; a clear increase in remyelinated axons in the dorsal funiculus could be shown in the S1PR2 KO as well as the JTE-013 treated mice. In lysolecithin injected optic nerves, a significant recovery of the optokinetic response could be demonstrated in the S1PR2 KO animals which was absent in the respective controls. Importantly, both S1PR2 KO EAE animals and EAE mice injected with JTE-013 from the day of the appearance of clinical signs showed a milder clinical course of EAE. Together, these findings reveal a new role for S1PR2 in the process of inflammation as well as repair of the CNS under conditions of demyelination and autoimmune attack. Regarding BBB extravasation, macrophage recruitment and, to a less degree, OPC differentiation the same results were obtained in both models of demyelination, indicating that the effects we saw were not model or inflammation dependent.

We found a higher number of newly formed mature oligodendrocytes in JTE-013 treated and in S1PR2 KO groups in comparison to the vehicle group at 16 dpi, whereas S1PR2 inactivation had no significant effect on proliferation and recruitment of OPCs in lysolecithin-induced demyelination. At the same time point, the ratio of labeled mature oligodendrocytes to labeled OPCs was higher in S1PR2 inactivated groups as compared to the vehicle group. Since at the earlier time point -i.e. 7 dpi- the population of labeled OPCs was not significantly different between the experimental groups, the difference in the number of labeled mature oligodendrocytes is probably due to an inhibitory effect of S1PR2 on differentiation. Such an effect could be direct or indirect. Myelin debris and oligodendrocyte exosomes were shown to inhibit OPCs differentiation and myelin formation by RhoA-ROCK signaling, the well-known downstream signaling molecules of NgR and S1PR2 (Baer et al., 2009; Bakhti et al., 2011; Schwab and Strittmatter, 2014). At 7 dpi double-immunostaining of PDGFRα and S1PR2 showed the expression of this receptor in OPCs (data not shown) and the presence of S1PR2 mRNA in primary OPCs culture was previously shown (Novgorodov et al., 2007). Therefore, S1PR2 could function as an inhibitor of OPC differentiation upon exposure to myelin debris. A direct inhibitory effect of S1PR2 inactivation on OPCs

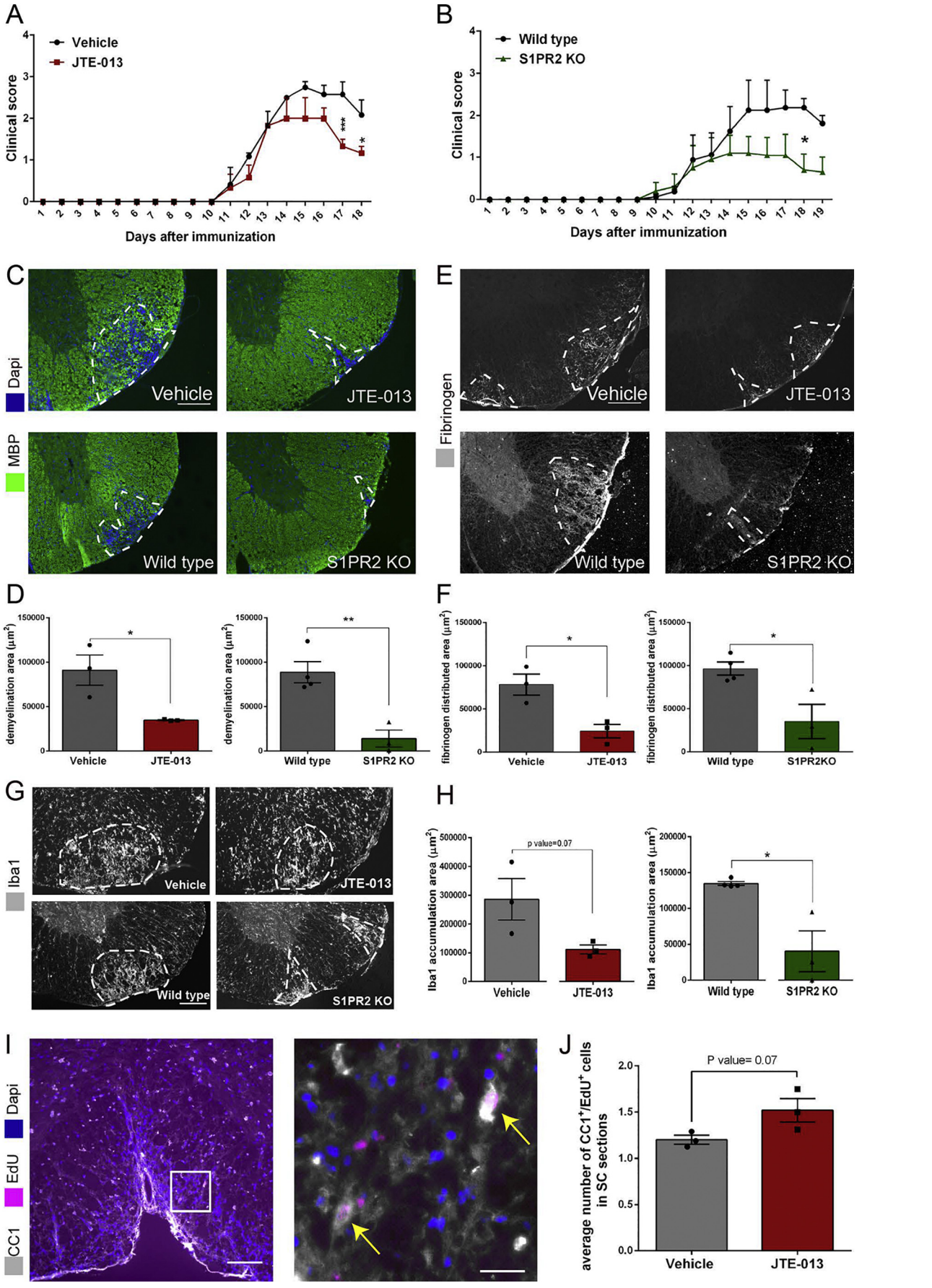

(caption on next page)

Fig. 5. S1PR2 inactivation deceases clinical score, spinal cord demyelination, BBB leakage, and macrophage/microglia numbers in EAE lesions and increases new oligodendrocyte generation in EAE mice. A, Clinical EAE score in JTE-013 treated mice in comparison to vehicle treated animals (two experiments with at least 3 mice per group). Daily JTE-013 injections were started from the first sign of disease and continued until the end of experiment. B, Clinical EAE score in Wild type (n = 4) and S1PR2 KO (n = 5) mice (For A and B, *p < .05, ***p < .001, repeated measured two-way ANOVA with Bonferroni post test). C and D, MBP/Dapi immunostaining in spinal cord revealing the demyelination areas (indicated by dashed line) and quantification of these areas in JTE-013, S1PR2 KO and control mice at 18–19 dpi. E and F, Fibrinogen immunostaining showing the sites of BBB leakage (indicated by dashed line) and the respective quantification of these areas at 18–19 dpi (For D and F, * p < .05 and **p < .01, n = 3 to 4 animals per group, student's *t*-test, scale bar for C and E = 150 μm). G, Immunostaining of Iba1 in spinal cord tissues from EAE mice at 18–19 dpi (scale bar = 150 μm). H, The graphs show the area of $Iba1^+$ cells accumulation in different parts of spinal cord (p = .07 and * p < .05, n = 3 to 4 animals per group, student's *t*-test). I, $CC1^+/EdU^+$ cells in the ventral white matter of spinal cord (right, scale bar = 100 μm) and two $CC1^+/EdU^+$ cells (arrow heads, left, scale bar = 20 μm). J, Quantification of $CC1^+/EdU^+$ cells in randomly chosen sections through the spinal cord (p = .07, n = 3 animals per group, student's *t*-test). The pictures shown in C and E are from thoracic segment and the pictures in G and I are from lumbar segment. Abbreviation: dpi = days post immunization.

differentiation is also in line with the role of NgR1 and its co-receptor Lingo1 in oligodendrocyte lineage cell differentiation (Mi et al., 2007; Sozmen et al., 2016). A related S1PR, S1PR5, was shown to have an inhibitory effect on oligodendrocyte differentiation and myelin formation as well (Jaillard et al., 2005). On the other hand, the presence of fibrinogen in CNS tissue e.g. after lysolecithin injection was also shown to suppress OPCs differentiation to oligodendrocytes and inhibit the remyelination (Petersen et al., 2017). Since at 3 dpi, we observed a decrease in the fibrinogen extravasation in S1PR2 inactivated groups, the later effect of S1PR2 inactivation on OPCs differentiation could also be related to the reduced fibrinogen load at earlier time points. Using S1PR2 conditional knockout mice for oligodendrocyte lineage can further elucidate the specific role of S1PR2 on these cells.

We observed a strong positive effect of S1PR2 inhibition or its genetic deletion on remyelination. This observation is in line with the effect of the direct Nogo-A inhibition on remyelination (Chong et al., 2012; Ineichen et al., 2017). The enhanced remyelination can partially be explained by the higher number of differentiated oligodendrocytes, but also by an effect of Nogo on myelinogenesis as described before (Chong et al., 2012). Chong and colleagues showed that the amino terminal part of Nogo-A decreases the myelin formation by an individual oligodendrocyte. Interestingly, the responsible receptor in this process remained unknown. As mature oligodendrocytes express S1PR2 (Yu et al., 2004), which can act as a receptor for Nogo-A (Kempf et al., 2014), it could be that Nogo-A decreases the myelinogenic potential through S1PR2. Furthermore, S1PR2 and Nogo-A signaling activate the RhoA/ROCK pathway and can mutually inhibit Rac1 (Ishii et al., 2010; Niederöst et al., 2002). RhoA/ROCK is known to negatively regulate CNS myelination, and Rac1 is important for correct myelin wrapping around axons (Thurnherr et al., 2006; Laura Feltri et al., 2008).

In the lysolecithin injection to optic chiasm, the visual acuity was higher in the S1PR2 KO group in comparison to control at 14 dpi. Similarly, there was an increasing trend in the JTE-013 injected group in comparison to the control group. It is shown that following lysolecithin injection in optic tract, the drop in the visual acuity is due to the failure in conduction and interestingly, boosting the conduction velocity by potassium channel blockers could compensate this failure (Bei et al., 2016). Remyelination may also increase the conduction velocity as it is shown by decreasing the delay caused by demyelination in VEP recordings. Since the number of the newly formed mature oligodendrocytes were higher in the JTE-013 treated group, it is possible that remyelination improved the visual acuity at 14 dpi.

In EAE, S1PR2 inhibition or genetic ablation decreased the clinical score as it was described before (Cruz-Orengo et al., 2014). This observation was concomitant with a decrease in the extent of BBB leakage and demyelination area in the S1PR2 inactivated groups. The decrease in the clinical score and demyelination area could in fact be partially caused by the reduced fibrinogen extravasation as fibrinogen can initiate inflammation, demyelination and microglial activation. Fibrinogen suppression ameliorated clinical scores in EAE mice (Adams et al., 2007; Ryu et al., 2015). In the lysolecithin model, the observed decrease in fibrinogen extravasation in S1PR2 KO and JTE-013 treated mice was not concomitant with a reduced extent of lesion volume and demyelination. This is in line with a recent study showing that lysolecithin induced demyelination is due mainly to a direct detergent effect of this compound on the myelin, leading to its destruction and subsequent removal (Plemel et al., 2018).

Analysis of the spinal cord tissue of EAE mice showed a reduction of the area in which $Iba1^+$ cells (including both CNS-dwelling microglia and monocyte-derived invading phagocytes) were accumulated. Since in EAE, monocytes act as important effector cells in tissue damage (Ajami et al., 2011), the decrease in the demyelination could also be due in part to reduced monocyte recruitment. Similar to EAE, in lysolecithin model S1PR2 inactivation decreased the number of $Iba1^+$ cells in the lesion area. Similar to our study, in an experimental model of atherosclerosis, the genetic ablation of S1PR2 was shown to reduce the load of the macrophages in lesions. Interestingly, the genetic ablation of S1PR2, didn't change the frequency of circulating immune cells in intact animals (Skoura et al., 2011). Our unpublished data also showed that in the EAE model, the frequency of monocytes, B lymphocytes and neutrophils were similar in JTE-013 treated and S1PR2 KO groups in comparison to their controls. Together, it seems that S1PR2 inactivation modulate the recruitment of $Iba1^+$ cells to injured tissue, while the frequencies of immune cells in plasma were unchanged.

S1P is the first described ligand for S1PR2. Nogo-A was also found to specifically bind to and activate this receptor (Kempf et al., 2014). Our previous studies demonstrated that many typical inhibitory effects of Nogo in vitro and in vivo are mediated via S1PR2 while S1P signaling can modulate these effects. S1P concentration in plasma is high and probably can affect endothelial cells and immune cells in blood through S1PR2. In the intact brain S1P content is relatively low (10 pmol/mg) (Kimura et al., 2008), while Nogo-A is abundant in white matter and can be expected to stimulate the S1PR2 in the brain. Following a BBB damage, S1P from the blood and from inflammatory cells enters the CNS tissue, suggesting a combined and synergistic activation of S1PR2 by S1P and Nogo-A. The present results do not allow to distinguish between S1P and Nogo-A induced S1PR2 activation in our experimental settings. However, the inhibitory role of Nogo-A on remyelination and behavioral outcome in EAE described earlier (Chong et al., 2012; Ineichen et al., 2017; Karnezis et al., 2004) suggests that S1PR2 has an important role as a Nogo-A receptor in this biological context.

Cruz-Orengo and colleagues, observed a higher expression of S1PR2 in the brain vasculature in female as compared to male SJL mice and showed that this is correlated with the higher susceptibility of females to EAE. Additionally, they showed that the well-studied effect of S1PR2 on BBB leakage is responsible for the higher susceptibility of females to EAE (Cruz-Orengo et al., 2014). On the other hand, the critical role of S1PR1 for the regulation of immune cells attracted significant attention to the role of S1PRs and S1PR modulating drugs for the treatment of MS. The functional antagonist of S1PR1 FTY720/Fingolimod suppresses the migration of lymphocytes out of lymphoid organs and therefore has strong protective effects in MS; the compound is one of the most widely used MS drugs today (Brinkmann et al., 2010). S1PR5, another receptor of the S1PR family, is expressed in all oligodendrocyte lineage cells and regulates OPCs migration and differentiation (Jaillard et al., 2005). One may ask about the potential compensatory role of S1PR5 or S1PR1 on

remyelination after ablation of the S1PR2 gene. We believe that this is not the case since we observed no changes in the amount of S1PR5 and S1PR1 mRNA in the CNS of S1PR2 KO animals in comparison to wild type littermates (data not shown). Additionally, almost the same effects as in the S1PR2 KO mice were observed in the animal groups that received JTE-013, a well characterized and widely used antagonist for S1PR2.

5. Conclusions

By using S1PR2 KO mice as well as pharmacological S1PR2 blockade, our findings show a dual beneficial effect of S1PR2 inactivation in demyelinating, MS-like lesions: better protection of the BBB against damage and smaller lesions on one hand, and enhanced oligodendrocyte differentiation and remyelination on the other hand. These results raise intriguing possibilities for selective S1PR2 blocking drugs as therapeutic agents in specific phases of MS.

Acknowledgments

M.S·S was supported by travel grants from the Iranian Ministry of Science, Research and Technology, as well as the Cognitive Sciences and Technologies Council of Iran, and MSIF's Du Pré Grant. The research project was supported by the European Research Council (ERC) advanced grant NOGORISE (294115), the Swiss National Science Foundation Grant Nr. 31003A-149315-1 (to M.E.S), PP00P3_144781 (to M.G), 310030_146130, 316030_150768, 310030_170320 (to B.B.), and the Spinal Cord Consortium of the Christopher and Dana Reeve Foundation (to M.E.S). M.J was supported by grants from Tarbiat Modares University and Royan Institute. The funding sources had no involvement in the study design, implementation, interpretation, or publication decisions. We cordially thank Dr. Michael Maurer for his critical advises through the study. We would like to thank Dr. Zorica Ristic, Kristin Skaar, and Diana Kukelova for their technical support.

Conflict of interest

M.E.S is a founder and board member of the University of Zurich spin-off company NovaGo Therapeutics Inc. seeking at developing antibody based therapies for neurological diseases.

Appendix A. Supplementary data

Supplementary data to this article can be found online at https://doi.org/10.1016/j.nbd.2018.11.018.

References

Adada, M., Canals, D., Hannun, Y.A., Obeid, L.M., 2013. Sphingosine-1-phosphate receptor 2. FEBS J. 280, 6354–6366. https://doi.org/10.1111/febs.12446.

Adams, R.A., Bauer, J., Flick, M.J., Sikorski, S.L., Nuriel, T., Lassmann, H., Degen, J.L., Akassoglou, K., 2007. The fibrin-derived $\gamma^{377-395}$ peptide inhibits microglia activation and suppresses relapsing paralysis in central nervous system autoimmune disease. J. Exp. Med. 204, 571–582. https://doi.org/10.1084/jem.20061931.

Ajami, B., Bennett, J.L., Krieger, C., McNagny, K.M., Rossi, F.M.V., 2011. Infiltrating monocytes trigger EAE progression, but do not contribute to the resident microglia pool. Nat. Neurosci. 14, 1142–1149. https://doi.org/10.1038/nn.2887.

Baer, A.S., Syed, Y.A., Kang, S.U., Mitteregger, D., Vig, R., Ffrench-Constant, C., Franklin, R.J.M., Altmann, F., Lubec, G., Kotter, M.R., 2009. Myelin-mediated inhibition of oligodendrocyte precursor differentiation can be overcome by pharmacological modulation of Fyn-RhoA and protein kinase C signalling. Brain 132, 465–481. https://doi.org/10.1093/brain/awn334.

Bakhti, M., Winter, C., Simons, M., 2011. Inhibition of myelin membrane sheath formation by oligodendrocyte-derived exosome-like vesicles. J. Biol. Chem. 286, 787–796. https://doi.org/10.1074/jbc.M110.190009.

Bei, F., Lee, H.H.C., Liu, X., Gunner, G., Jin, H., Ma, L., Wang, C., Hou, L., Hensch, T.K., Frank, E., Sanes, J.R., Chen, C., Fagiolini, M., He, Z., 2016. Restoration of visual function by enhancing conduction in regenerated axons. Cell 164, 219–232. https://doi.org/10.1016/j.cell.2015.11.036.

Brinkmann, V., Billich, A., Baumruker, T., Heining, P., Schmouder, R., Francis, G., Aradhye, S., Burtin, P., 2010. Fingolimod (FTY720): discovery and development of an oral drug to treat multiple sclerosis. Nat. Rev. Drug Discov. 9, 883–897. https://doi.org/10.1038/nrd3248.

Chong, S.Y.C., Rosenberg, S.S., Fancy, S.P.J., Zhao, C., Shen, Y.-A.A., Hahn, A.T., McGee, A.W., Xu, X., Zheng, B., Zhang, L.I., Rowitch, D.H., Franklin, R.J.M., Lu, Q.R., Chan, J.R., 2012. Neurite outgrowth inhibitor Nogo-A establishes spatial segregation and extent of oligodendrocyte myelination. Proc. Natl. Acad. Sci. 109, 1299–1304. https://doi.org/10.1073/pnas.1113540109.

Cruz-Orengo, L., Daniels, B.P., Dorsey, D., Basak, S.A., Grajales-Reyes, J.G., McCandless, E.E., Piccio, L., Schmidt, R.E., Cross, A.H., Crosby, S.D., Klein, R.S., 2014. Enhanced sphingosine-1-phosphate receptor 2 expression underlies female CNS autoimmunity susceptibility. J. Clin. Invest. 124, 2571–2584. https://doi.org/10.1172/JCI73408.

Deshmukh, V.A., Tardif, V., Lyssiotis, C.A., Green, C.C., Kerman, B., Kim, H.J., Padmanabhan, K., Swoboda, J.G., Ahmad, I., Kondo, T., Gage, F.H., Theofilopoulos, A.N., Lawson, B.R., Schultz, P.G., Lairson, L.L., 2013. A regenerative approach to the treatment of multiple sclerosis. Nature 502, 327–332. https://doi.org/10.1038/nature12647.

Duncan, I.D., Marik, R.L., Broman, A.T., Heidari, M., 2017. Thin myelin sheaths as the hallmark of remyelination persist over time and preserve axon function. Proc. Natl. Acad. Sci. 201714183.

Ferent, J., Zimmer, C., Durbec, P., Ruat, M., Traiffort, E., 2013. Sonic hedgehog signaling is a positive oligodendrocyte regulator during demyelination. J. Neurosci. 33, 1759–1772. https://doi.org/10.1523/JNEUROSCI.3334-12.2013.

Franklin, R.J.M., Ffrench-Constant, C., 2017. Regenerating CNS myelin — from mechanisms to experimental medicines. Nat. Rev. Neurosci. 18, 753–769. https://doi.org/10.1038/nrn.2017.136.

Green, A.J., Gelfand, J.M., Cree, B.A., Bevan, C., Boscardin, W.J., Mei, F., Inman, J., Arnow, S., Devereux, M., Abounasr, A., Nobuta, H., Zhu, A., Friessen, M., Gerona, R., Von Budingen, H.C., Henry, R.G., Hauser, S.L., Chan, J.R., 2017. Articles clemastine fumarate as a remyelinating therapy for multiple sclerosis (ReBUILD): a randomised, controlled, double-blind, crossover trial 6736. https://doi.org/10.1016/S0140-6736(17)32346-2.

Huang, F., Mehta, D., Predescu, S., Kim, K., Lum, H., 2007. A novel lysophospholipid- and pH-sensitive receptor, GPR4, in brain endothelial cells regulates monocyte transmigration. Endothel. J. Endothel. Cell Res. 14, 25–34. https://doi.org/10.1080/10623320601177288.

Ineichen, B.V., Weinmann, O., Good, N., Plattner, P., Wicki, C., Rushing, E.J., Linnebank, M., Schwab, M.E., 2016. Sudan black: a fast, easy, and non-toxic method to assess myelin repair in demyelinating diseases. Neuropathol. Appl. Neurobiol. 242–251. https://doi.org/10.1111/nan.12373.

Ineichen, B.V., Kapitza, S., Bleul, C., Good, N., Plattner, P.S., Seyedsadr, M.S., Kaiser, J., Schneider, M.P., Zörner, B., Martin, R., Linnebank, M., Schwab, M.E., 2017. Nogo-A antibodies enhance axonal repair and remyelination in neuro-inflammatory and demyelinating pathology. Acta Neuropathol. 134, 423–440. https://doi.org/10.1007/s00401-017-1745-3.

Ishii, M., Kikuta, J., Shimazu, Y., Meier-Schellersheim, M., Germain, R.N., 2010. Chemorepulsion by blood S1P regulates osteoclast precursor mobilization and bone remodeling in vivo. J. Exp. Med. 207, 2793–2798. https://doi.org/10.1084/jem.20101474.

Jaillard, C., Harrison, S., Stankoff, B., Aigrot, M.S., Calver, A.R., Duddy, G., Walsh, F.S., Pangalos, M.N., Arimura, N., Kaibuchi, K., Zalc, B., Lubetzki, C., 2005. Edg8/S1P5: an oligodendroglial receptor with dual function on process retraction and cell survival. J. Neurosci. 25, 1459–1469. https://doi.org/10.1523/JNEUROSCI.4645-04.2005.

Karnezis, T., Mandemakers, W., McQualter, J.L., Zheng, B., Ho, P.P., Jordan, K. a, Murray, B.M., Barres, B., Tessier-Lavigne, M., Bernard, C.C. a, 2004. The neurite outgrowth inhibitor Nogo A is involved in autoimmune-mediated demyelination. Nat. Neurosci. 7, 736–744. https://doi.org/10.1038/nn1261.

Kempf, A., Tews, B., Arzt, M.E., Weinmann, O., Obermair, F.J., Pernet, V., Zagrebelsky, M., Delekate, A., Iobbi, C., Zemmar, A., Ristic, Z., Gullo, M., Spies, P., Dodd, D., Gygax, D., Korte, M., Schwab, M.E., 2014. The sphingolipid receptor S1PR2 is a receptor for nogo-A Repressing synaptic plasticity. PLoS Biol. 12, e1001763. https://doi.org/10.1371/journal.pbio.1001763.

Kim, G.S., Yang, L., Zhang, G., Zhao, H., Selim, M., McCullough, L.D., Kluk, M.J., Sanchez, T., 2015. Critical role of sphingosine-1-phosphate receptor-2 in the disruption of cerebrovascular integrity in experimental stroke. Nat. Commun. 6, 7893. https://doi.org/10.1038/ncomms8893.

Kimura, A., Ohmori, T., Kashiwakura, Y., Ohkawa, R., Madoiwa, S., Mimuro, J., Shimazaki, K., Hoshino, Y., Yatomi, Y., Sakata, Y., 2008. Antagonism of sphingosine 1-phosphate receptor-2 enhances migration of neural progenitor cells toward an area of brain infarction. Stroke 39, 3411–3417. https://doi.org/10.1161/STROKEAHA.108.514612.

Kono, M., Mi, Y., Liu, Y., Sasaki, T., Allende, M.L., Wu, Y.P., Yamashita, T., Proia, R.L., 2004. The sphingosine-1-phosphate receptors S1P1, S1P2, and S1P3 function coordinately during embryonic angiogenesis. J. Biol. Chem. 279, 29367–29373. https://doi.org/10.1074/jbc.M403937200.

Laura Feltri, M., Suter, U., Relvas, J.B., 2008. The function of rhogtpases in axon ensheathment and myelination. Glia 56, 1508–1517. https://doi.org/10.1002/glia.20752.

Mellion, M., Edwards, K.R., Hupperts, R., Drulović, J., Montalban, X., Hartung, H.-P., Brochet, B., Calabresi, P.A., Rudick, R., Ibrahim, A., Zhang, Y., Xu, L., Cadavid, D., 2017. Efficacy results from the phase 2b SYNERGY Study: treatment of disabling multiple sclerosis with the anti-LINGO-1 monoclonal antibody opicinumab (S33.004). Neurology 88 (S33.004).

Mi, S., Hu, B., Hahm, K., Luo, Y., Kam Hui, E.S., Yuan, Q., Wong, W.M., Wang, L., Su, H., Chu, T.-H., Guo, J., Zhang, W., So, K.-F., Pepinsky, B., Shao, Z., Graff, C., Garber, E., Jung, V., Wu, E.X., Wu, W., 2007. LINGO-1 antagonist promotes spinal cord remyelination and axonal integrity in MOG-induced experimental autoimmune

encephalomyelitis. Nat. Med. 13, 1228–1233. https://doi.org/10.1038/nm1664.
Miron, V.E., Ludwin, S.K., Darlington, P.J., Jarjour, A.A., Soliven, B., Kennedy, T.E., Antel, J.P., 2010. Fingolimod (FTY720) enhances remyelination following demyelination of organotypic cerebellar slices. Am. J. Pathol. 176, 2682–2694. https://doi.org/10.2353/ajpath.2010.091234.
Miron, V.E., Boyd, A., Zhao, J.-W., Yuen, T.J., Ruckh, J.M., Shadrach, J.L., van Wijngaarden, P., Wagers, A.J., Williams, A., Franklin, R.J.M., French-Constant, C., 2013. M2 microglia and macrophages drive oligodendrocyte differentiation during CNS remyelination. Nat. Neurosci. 16, 1211–1218. https://doi.org/10.1038/nn.3469.
Najm, F.J., Madhavan, M., Zaremba, A., Shick, E., Karl, R.T., Factor, D.C., Miller, T.E., Nevin, Z.S., Kantor, C., Sargent, A., Quick, K.L., Schlatzer, D.M., Tang, H., Papoian, R., Brimacombe, K.R., Shen, M., Boxer, M.B., Jadhav, A., Robinson, A.P., Podojil, J.R., Miller, S.D., Miller, R.H., Tesar, P.J., 2015. Drug-based modulation of endogenous stem cells promotes functional remyelination in vivo. Nature 522, 216–220. https://doi.org/10.1038/nature14335.
Niederöst, B., Oertle, T., Fritsche, J., McKinney, R.A., Bandtlow, C.E., 2002. Nogo-A and myelin-associated glycoprotein mediate neurite growth inhibition by antagonistic regulation of RhoA and Rac1. J. Neurosci. 22, 10368–10376 (22/23/10368-76).
Novgorodov, A.S., El-Alwani, M., Bielawski, J., Obeid, L.M., Gudz, T.I., 2007. Activation of sphingosine-1-phosphate receptor S1P5 inhibits oligodendrocyte progenitor migration. FASEB J. 21, 1503–1514. https://doi.org/10.1096/fj.06-7420com.
Osada, M., Yatomi, Y., Ohmori, T., Ikeda, H., Ozaki, Y., 2002. Enhancement of sphingosine 1-phosphate-induced migration of vascular endothelial cells and smooth muscle cells by an EDG-5 antagonist. Biochem. Biophys. Res. Commun. 299, 483–487. https://doi.org/10.1016/S0006-291X(02)02671-2.
Petersen, M.A., Ryu, J.K., Chang, K.-J., Etxeberria, A., Bardehle, S., Mendiola, A.S., Kamau-Devers, W., Fancy, S.P.J., Thor, A., Bushong, E.A., Baeza-Raja, B., Syme, C.A., Wu, M.D., Rios Coronado, P.E., Meyer-Franke, A., Yahn, S., Pous, L., Lee, J.K., Schachtrup, C., Lassmann, H., Huang, E.J., Han, M.H., Absinta, M., Reich, D.S., Ellisman, M.H., Rowitch, D.H., Chan, J.R., Akassoglou, K., 2017. Fibrinogen activates BMP signaling in oligodendrocyte progenitor cells and inhibits remyelination after vascular damage. Neuron 1–10. https://doi.org/10.1016/j.neuron.2017.10.008.
Petratos, S., Ozturk, E., Azari, M.F., Kenny, R., Young Lee, J., Magee, K.A., Harvey, A.R., McDonald, C., Taghian, K., Moussa, L., Mun Aui, P., Siatskas, C., Litwak, S., Fehlings, M.G., Strittmatter, S.M., Bernard, C.C.A., 2012. Limiting multiple sclerosis related axonopathy by blocking Nogo receptor and CRMP-2 phosphorylation. Brain 135, 1794–1818. https://doi.org/10.1093/brain/aws100.
Plemel, J.R., Michaels, N.J., Weishaupt, N., Caprariello, A.V., Keough, M.B., Rogers, J.A., Yukseloglu, A., Lim, J., Patel, V.V., Rawji, K.S., Jensen, S.K., Teo, W., Heyne, B., Whitehead, S.N., Stys, P.K., Yong, V.W., 2018. Mechanisms of lysophosphatidylcholine-induced demyelination: a primary lipid disrupting myelinopathy. Glia 66, 327–347. https://doi.org/10.1002/glia.23245.
Pourabdolhossein, F., Mozafari, S., Morvan-Dubois, G., Mirnajafi-Zadeh, J., Lopez-Juarez, A., Pierre-Simons, J., Demeneix, B.A., Javan, M., 2014. Nogo receptor inhibition enhances Functional recovery following lysolecithin-induced demyelination in mouse optic chiasm. PLoS One 9. https://doi.org/10.1371/journal.pone.0106378.
Prusky, G.T., Alam, N.M., Beekman, S., Douglas, R.M., 2004. Rapid quantification of adult and developing mouse spatial vision using a virtual optomotor system. Investig. Ophthalmol. Vis. Sci. 45, 4611–4616. https://doi.org/10.1167/iovs.04-0541.
Qiao, J., Huang, F., Naikawadi, R.P., Kim, K.S., Said, T., Lum, H., 2006. Lysophosphatidylcholine impairs endothelial barrier function through the G protein-coupled receptor GPR4. Am. J. Physiol. Lung Cell Mol. Physiol. 291, L91–101. https://doi.org/10.1152/ajplung.00508.2005.
Ransohoff, R.M., Hafler, D.A., Lucchinetti, C.F., 2015. Multiple sclerosis—a quiet revolution. Nat. Rev. Neurol. 11, 134–142. https://doi.org/10.1038/nrneurol.2015.14.
Rawji, K.S., Yong, V.W., 2013. The benefits and detriments of macrophages/microglia in models of multiple sclerosis. Clin. Dev. Immunol. 2013, 1–13.
Ryu, J.K., Petersen, M.A., Murray, S.G., Baeten, K.M., Meyer-Franke, A., Chan, J.P., Vagena, E., Bedard, C., Machado, M.R., Coronado, P.E.R., Prod'homme, T., Charo, I.F., Lassmann, H., Degen, J.L., Zamvil, S.S., Akassoglou, K., 2015. Blood coagulation protein fibrinogen promotes autoimmunity and demyelination via chemokine release and antigen presentation. Nat. Commun. 6, 8164. https://doi.org/10.1038/ncomms9164.
Salic, A., Mitchison, T.J., 2008. A chemical method for fast and sensitive detection of DNA synthesis in vivo. Proc. Natl. Acad. Sci. U. S. A. 105, 2415–2420. https://doi.org/10.1073/pnas.0712168105.
Schwab, M.E., Strittmatter, S.M., 2014. Nogo limits neural plasticity and recovery from injury. Curr. Opin. Neurobiol. 27, 53–60. https://doi.org/10.1016/j.conb.2014.02.011.
Skoura, A., Michaud, J., Im, D.S., Thangada, S., Xiong, Y., Smith, J.D., Hla, T., 2011. Sphingosine-1-phosphate receptor-2 function in myeloid cells regulates vascular inflammation and atherosclerosis. Arterioscler. Thromb. Vasc. Biol. 31, 81–85. https://doi.org/10.1161/ATVBAHA.110.213496.
Sozmen, E.G., Rosenzweig, S., Llorente, I.L., Ditullio, D.J., Machnicki, M., Vinters, H.V., Havton, L.A., Giger, R.J., Hinman, J.D., Carmichael, S.T., 2016. Nogo receptor blockade overcomes remyelination failure after white matter stroke and stimulates functional recovery in aged mice. Proc. Natl. Acad. Sci. 201615322. https://doi.org/10.1073/pnas.1615322113.
Thurnherr, T., Benninger, Y., Wu, X., Chrostek, A., Krause, S.M., Nave, K.-A., Franklin, R.J.M., Brakebusch, C., Suter, U., Relvas, J.B., 2006. Cdc42 and Rac1 signaling are both required for and act synergistically in the correct formation of myelin sheaths in the CNS. J. Neurosci. 26, 10110–10119. https://doi.org/10.1523/JNEUROSCI.2158-06.2006.
Wegener, A., Deboux, C., Bachelin, C., Frah, M., Kerninon, C., Seilhean, D., Weider, M., Wegner, M., Nait-Oumesmar, B., 2015. Gain of Olig2 function in oligodendrocyte progenitors promotes remyelination. Brain 138, 120–135. https://doi.org/10.1093/brain/awu375.
Yang, Y., Liu, Y., Wei, P., Peng, H., Winger, R., Hussain, R.Z., Ben, L.H., Cravens, P.D., Gocke, A.R., Puttaparthi, K., Racke, M.K., McTigue, D.M., Lovett-Racke, A.E., 2010. Silencing Nogo-A promotes functional recovery in demyelinating disease. Ann. Neurol. 67, 498–507. https://doi.org/10.1002/ana.21935.
Yazdi, A., Baharvand, H., Javan, M., 2015. Enhanced remyelination following lysolecithin-induced demyelination in mice under treatment with fingolimod (FTY720). Neuroscience 311, 34–44. https://doi.org/10.1016/j.neuroscience.2015.10.013.
Yu, N., Lariosa-Willingham, K.D., Lin, F.F., Webb, M., Rao, T.S., 2004. Characterization of lysophosphatidic acid and sphingosine-1-phosphate-mediated signal transduction in rat cortical oligodendrocytes. Glia 45, 17–27. https://doi.org/10.1002/glia.10297.